Modeling of Grid-Forming and Grid-Following Inverters for Transient Stability Simulation of Large-Scale Distribution Systems

Wei Du, *Member, IEEE*, Francis K. Tuffner, *Member*, Kevin P. Schneider, *Senior Member, IEEE*, Robert H. Lasseter, *Life Fellow, IEEE*, Jing Xie, *Member, IEEE*, Zhe Chen, *Student Member, IEEE*, and Bishnu Bhattarai, *Senior Member, IEEE*

***Abstract*—Traditional dynamic models of inverter-based DERs are mostly electromagnetic models and positive-sequence electromechanical models, neither of which is suitable for simulation of large-scale, three-phase unbalanced distribution systems. This paper develops three-phase, electromechanical models for both grid-forming and grid-following inverters, and integrates them into a three-phase unbalanced distribution network solver, enabling transient stability simulation of large-scale distribution systems with high penetration of inverter-based DERs. The proposed inverter models are validated against electromagnetic simulations and field test data from the CERTS/AEP microgrid testbed, and simulated in an islanded 5,252 node distribution system in the GridLAB-D simulation environment. Simulation verifies the effectiveness of the proposed models for large-scale distribution systems. Results show that compared to grid-following inverters, the high penetration of grid-forming inverters can significantly improve the voltage and frequency transient stability of distribution systems.**

***Index Terms*—Inverter, grid-forming, grid-following, transient stability, modeling, distribution systems**

I. Introduction

POWER systems are undergoing a major transition with increasing penetrations of distributed energy resources (DERs) connected at the distribution level, including both synchronous generator-based and inverter-based DERs [1, 2]. Historically, distribution systems seldom have transient stability issues because of the existence of a strong substation voltage source and the limited number of DERs. However, the emerging generation of resilient distribution systems is expected to have the capability to allow portions of, or even all the distribution feeder to work in islanded modes when the substation voltage source is lost caused by events like extreme weather and natural disasters [3, 4]. For such islanded distribution systems with high penetration of DERs, transiently stability becomes an operational concern.

The Pacific Northwest National Laboratory is operated by Battelle for the U.S. Department of Energy under Contract DE-AC05-76RL01830.

W. Du, J. Xie, B. Bhattarai are with Pacific Northwest National Laboratory, Richland, WA 99354 USA (e-mail: wei.du@pnnl.gov, jing.xie@pnnl.gov, bishnu.bhattarai@pnnl.gov).

K. P. Schneider and F. K. Tuffner are with Pacific Northwest National Laboratory, Seattle Research Center, Seattle, WA 98109 USA (e-mail: kevin.schneider@pnnl.gov and francis.tuffner@pnnl.gov).

R. H. Lasseter and Z. Chen are with the Department of Electrical and Computer Engineering, University of Wisconsin-Madison, Madison, WI 53706-1691 USA (e-mail: Lasseter@engr.wisc.edu and zchen275@wisc.edu).

The transient stability of bulk power systems is dominated by large synchronous generators with high rotational inertia. In contrast, the transient stability of islanded distribution systems needs to be maintained by both synchronous generator-based and inverter-based DERs, whose stability characteristics could be very different than those of bulk power systems. The dynamics of synchronous generators are well understood and different dynamic models have been developed during past decades [5]. The work in [6] proposes a dynamic model of synchronous generators for transient stability simulation of distribution systems. However, inverter models for the transient stability simulation of distribution systems are lacking. Existing dynamic models of inverter-based DERs are mostly electromagnetic models and positive-sequence electromechanical models, neither of which works for large-scale, three-phase unbalanced distribution systems. The electromagnetic models can be used to evaluate the performance of a single inverter controller, but their use in simulating large-scale distribution systems, which typically have thousands of nodes in North America, is not practical. Positive-sequence electromechanical models are typically used for large-scale transmission systems studies. The work in [7-9] develop different positive-sequence models of inverters and investigate their impacts on the transient stability of bulk power systems. However, positive-sequence models cannot be applied to distribution systems due to the potentially unbalanced design and operations of distribution systems [10].

From the controller design perspective, inverter controls can be classified as one of two basic types: grid-following and grid-forming [1]. Grid-following control is widely used for grid-connected inverters. It makes the inverter behave approximately like a current source. In recent years, studies have shown that as the penetration of grid-following inverters increases in bulk power systems, with a corresponding decrease in synchronous generators, the system transient stability will be harmed [11, 12]. In contrast, grid-forming control is considered an emerging technology for power systems [13] that typically makes the inverter behave like a voltage source. Different grid-forming controls have been proposed in recent years, and their capabilities to maintain transient stability have been verified in small-scale systems [14-19]. However, the impacts of grid-following and grid-forming inverters on large-scale distribution systems have not been investigated because of the lack of appropriate models.

This paper develops three-phase, electromechanical models for both grid-following and grid-forming inverters, and integrates them into a three-phase unbalanced distribution network solver, enabling the transient stability simulation of large-scale distribution systems with high penetration of inverter-based DERs. The proposed inverter models are validated against electromagnetic transient simulations and field test data from the Consortium for Electric Reliability Technology Solutions (CERTS)/American Electric Power (AEP) microgrid testbed [19], and evaluated in an islanded 5,252 node distribution feeder which has multiple synchronous generator-based and inverter-based DERs in the GridLAB-D simulation environment [20]. Simulation verifies the effectiveness of the proposed inverter models for large-scale distribution system studies. Study results show that, compared to grid-following inverters, the high penetration of grid-forming inverters can significantly improve the voltage and frequency transient stability of large-scale distribution systems.

II. Inertia of Synchronous Generators

A synchronous generator behaves approximately like a voltage source behind its subtransient reactance X_d'' during load transients, as shown in Fig. 1 [5]. During a load step, the generator draws necessary currents to meet any load changes, while its internal voltage E_d'' remains constant. However, the prime mover of a synchronous generator usually responds slowly [5]. This results in an imbalance between the generator's electrical power P_e and mechanical power P_m, forcing the rotor speed to change, as shown in Fig. 2. Equation (1) describes the swing equation of a synchronous generator, where H is the inertia constant and ω is the rotor speed. A larger H results in a smaller rate of speed change.

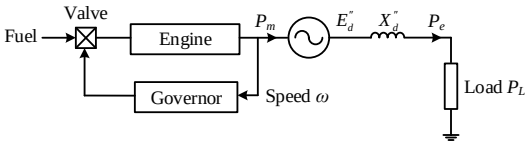

Fig. 1. Generator supplying isolated load.

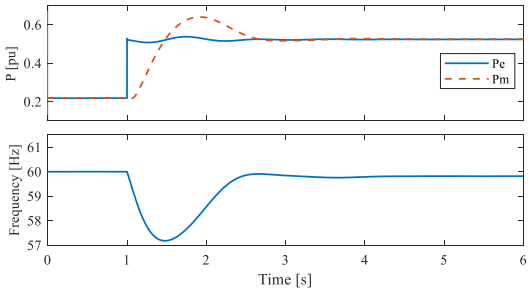

Fig. 2. Response of a synchronous generator to a load step.

$$2H\frac{d\omega}{dt} = P_m - P_e \tag{1}$$

Although the inertia constant H is important to maintain the frequency stability of a synchronous generator, a more fundamental reason for the frequency change is the imbalance between P_m and P_e during load transients caused by the slow response of P_m.

In a highly inverter-penetrated distribution system, if the inverter-based DERs could quickly respond to any load disturbances, the imbalance between P_m and P_e of synchronous generators could be reduced, helping to improve the frequency stability. The following sections introduce two typical inverter controls and discuss their different responses to load disturbances.

III. Inverter Controls

Most inverter-based DERs use the two-level, three-phase voltage source inverter, as shown in Fig. 3 [21]. Although the device is called a "voltage source" inverter, different control strategies can cause different dynamic behaviors of inverters. This section introduces two basic types of controls, known as "grid-following" and "grid-forming."

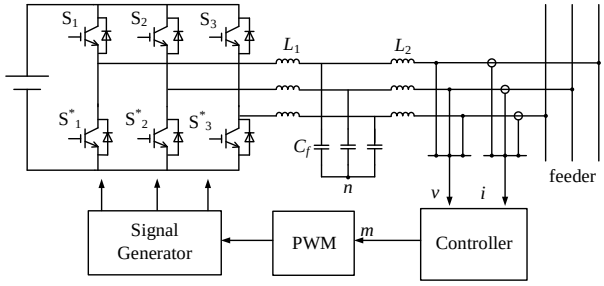

Fig. 3. A typical two-level, three-phase voltage source inverter.

A. Grid-Following Concept

Currently, most grid-connected, inverter-based DERs use grid-following control, which typically uses a phase-lock-loop (PLL) and a current control loop to achieve fast control of the inverter's output currents [21]. Grid-following control makes the voltage source inverter behave approximately like a current source, as shown in Fig. 4 (a). The advantage of this control is that the currents can be quickly regulated. However, because grid-following control does not control the voltage and frequency, it relies on an external voltage source to provide the voltage and frequency references. During load disturbances, grid-following inverters maintain their output power approximately constant.

B. Grid-Forming Concept

In contrast, grid-forming control controls the voltage and frequency of the inverter, making the voltage source inverter behave approximately like a voltage source, as shown in Fig. 4 (b). Because the voltage and frequency remain constant, the grid-forming inverters can work in stand-alone modes and track the loads [15]. To achieve parallel operation of multiple grid-forming inverters, different control strategies have been proposed, including droop control [14, 15], virtual oscillator control [16], and virtual synchronous machines [17], etc.

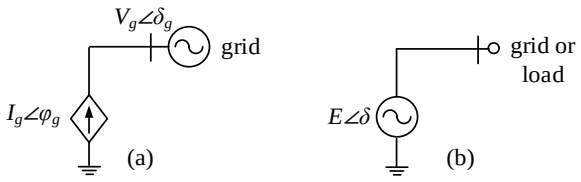

Fig. 4. Inverter controls: (a) grid-following and (b) grid-forming.

IV. Modeling of Inverters for Transient Stability Simulation of Large-Scale Distribution Systems

To investigate the impact of grid-following and grid-forming inverters on the transient stability of distribution systems, appropriate dynamic models need to be developed. This section introduces three-phase, electromechanical models of both grid-following and grid-forming inverters, and their interfaces to the distribution network solver.

A. Inverter Equivalent Circuit

The inverter main circuit in Fig. 3 can be modeled as a three-phase controllable voltage source behind the coupling reactance X_L, as shown in Fig. 5. The X_L accounts for the inverter's filter reactances L_1 and L_2. In this paper, the value of X_L is set as 0.1 pu on an inverter rating base. Filter capacitance C_f is ignored due to its small value in fundamental frequency. As shown in Fig. 5, the inputs of the controller are the three-phase terminal voltage $V_{gi}\angle\delta_{gi}$ (i=a,b,c) and current $I_{gi}\angle\varphi_{gi}$, and the outputs of the controller are the three-phase inverter internal voltage $E_i\angle\delta_i$. The controller can be either grid-following or grid-forming.

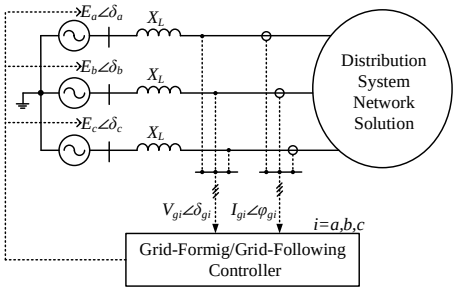

Fig. 5. Inverter equivalent circuit and controller.

To be linked with a distribution network solver, the circuit is converted to its Norton equivalence, as shown in Fig. 6 (a) and (b). The three-phase internal current $\dot{I}_{Ii}$ and the admittance Y_L can be calculated using (2) and (3).

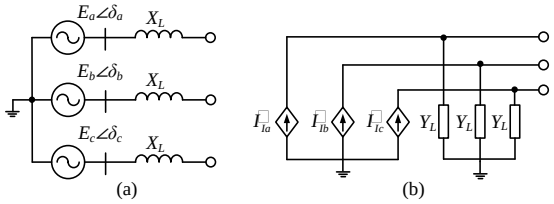

Fig. 6. Inverter equivalent circuits: (a) Thevenin equivalent circuit and (b) Norton equivalent circuit.

$$\dot{I}_{Ii} = \frac{E_i\angle\delta_i}{j\omega X_L}, \quad i = a,b,c \tag{2}$$

$$Y_L = \frac{1}{X_L} \tag{3}$$

B. Grid-Following Control Dynamic Model

In most commercially available transient stability simulation tools, the grid-following inverters are modeled as controllable PQ nodes, and the inner control loops are ignored [22, 23]. This paper instead seeks to faithfully represent the real control strategies used in grid-following inverters. Therefore, the two key components of grid-following control—PLL and current control loop, are modeled. Fig. 7 and Fig. 8 show the control blocks of a typical synchronous reference frame PLL and a typical current control loop, respectively. The control objective of the PLL is to estimate the phase angle of the grid voltage. As shown in Fig. 7 (a), the PLL uses a proportional-integral (PI) controller to control the component of the grid voltage on q-axis, v_{gqi}, to be zero by increasing or decreasing the virtual angular frequency $\Delta\omega_i$. The integration of $\Delta\omega_i$ is the estimated phase angle δ_{PLLi}. δ_{PLLi} should equal δ_{gi} in the steady state. Fig. 7 (b) illustrates how the PLL tracks the phase angle of the grid voltage. k_{pPLL} and k_{iPLL} are the proportional and integral gains of the controller.

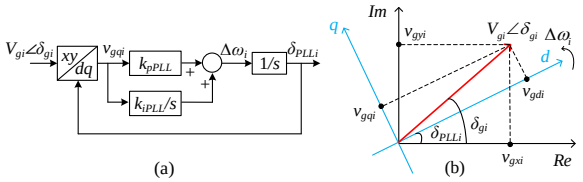

Fig. 7. PLL: (a) control block and (b) xy and dq frame coordinate systems.

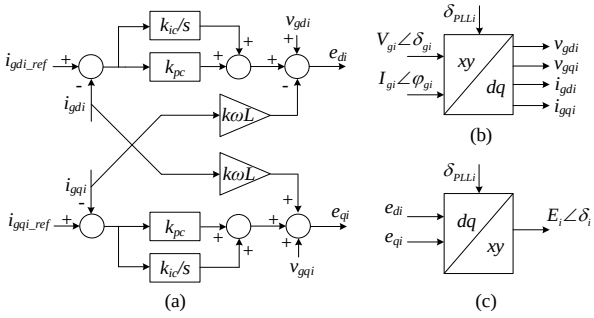

Fig. 8. Control block of the current control loop: (a) current loop, (b) and (c) coordinate transformation.

The current control loop quickly regulates the active and reactive currents injected into the grid by adjusting the inverter internal voltage $E_i\angle\delta_i$ rapidly. In this study, the output current of each phase is independently controlled in the dq frame through the PI controller, as shown in Fig. 8 (a). The grid voltage $V_{gi}\angle\delta_{gi}$ and current $I_{gi}\angle\varphi_{gi}$ are transferred from the xy frame to the dq frame based on the phase angle δ_{PLLi} obtained from the PLL, as shown in Fig. 8 (b). The outputs of the current loop are the inverter internal voltages in the dq frame, e_{di} and e_{qi}. To be linked with a three-phase power flow solver, e_{di} and e_{qi} are transferred from the dq frame to the xy frame, as shown in Fig. 8 (c). The grid-following inverters have the flexibility to inject either positive, negative, or zero sequence currents, but in this study they are controlled to only inject positive-sequence currents into distribution systems. The reference current, $\dot{I}_{gi\_ref}$, is calculated using (4) and (5), where $\dot{V}_{g1}$ is the positive-sequence voltage of the grid voltage, $\dot{I}_{g1\_ref}$ is the positive-sequence current reference of the inverter, P_{ref} and Q_{ref} are the references of active and reactive power, and α=e$^{j2\pi/3}$. The current reference $\dot{I}_{gi\_ref}$ is transferred to the dq frame to obtain the current references i_{gdi_ref} and i_{gqi_ref} shown in Fig. 8 (a). k_{pc} and k_{ic} are the gains of the current control loop.

$$\dot{I}_{g1\_ref} = \left(\frac{P_{ref} + jQ_{ref}}{\dot{V}_{g1}}\right)^* \tag{4}$$

$$\dot{I}_{ga\_ref} = \dot{I}_{g1\_ref},\ \dot{I}_{gb\_ref} = \alpha^2\dot{I}_{g1\_ref},\ \dot{I}_{gc\_ref} = \alpha\dot{I}_{g1\_ref} \tag{5}$$

Note that in recent years, different auxiliary controls have been proposed for grid-following inverters, aiming to provide voltage and frequency support to power systems, such as volt-var, frequency-watt, synthetic inertia, etc. [24, 25]. These controllers are designed as outer control loops that modify P_{ref} and Q_{ref}. The outer control loops are subject to the bandwidth of the inner control loops, so their responses are usually slow. The analysis and experimental results in [25] show that a first-order low-pass filter with a time constant of 1 s is needed for synthetic inertia control to guarantee local stability. The work in [8] indicates the slow response of frequency-watt control leads to a poor frequency response of bulk power systems. The grid support functions of grid-following inverters are not modeled in this paper. Instead, this study focuses on modeling detailed inner control loops of grid-following inverters, with future work examining different outer controls.

C. Grid-Forming Control Dynamic Model

As discussed in Section III-B, different grid-forming controls have been proposed in recent years. In this study, CERTS droop control was selected, because extensive field tests have been conducted at the CERTS/AEP microgrid test bed during the past decade [19], so it can be considered a relatively matured technology. As shown in Fig. 9 (a) and (b), CERTS droop control controls the voltage magnitude E and frequency f of the inverter internal voltage $E\angle\delta$ according to the Q-V droop control and P-f droop control, respectively, where m_q and m_p are the droop gains. The Q-V droop control avoids circulating reactive power between grid-forming inverters, and P-f droop control synchronizes the inverters and enables power sharing between them. In addition, overload mitigation control [26] is added to the P-f droop control to (a) prevent the output power of inverters from exceeding the maximum P_{max} or dropping below the minimum P_{min} during partial overload events in a microgrid, and (b) trigger under-frequency load shedding when all sources in a microgrid are overloaded. k_{pv} and k_{iv} are the gains of the voltage control loop. k_{ppmax} and k_{ipmax} are the gains of the overload mitigation control, and ω_0 is the rated angular frequency.

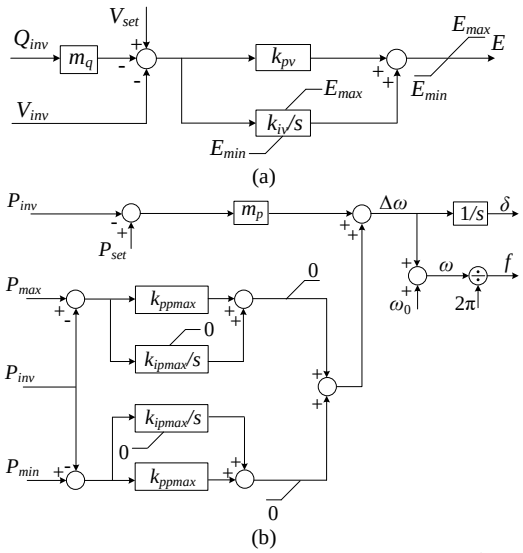

Fig. 9. CERTS Droop Control: (a) Q-V droop control and (b) P-f droop control and overload mitigation control.

The controller is linked to a three-phase network solver. The active power P_{inv} and reactive power Q_{inv} in Fig. 9 refer to the sum of the inverter three-phase output power. The voltage V_{inv} is the average value of the inverter three-phase terminal voltages. The calculations of P_{inv}, Q_{inv}, and V_{inv} are shown in (6) and (7), where T is the time constant of the low-pass filter.

$$P_{inv}=\frac{1}{1+Ts}(P_a+P_b+P_c)\ ,\ Q_{inv}=\frac{1}{1+Ts}(Q_a+Q_b+Q_c) \tag{6}$$

$$V_{inv}=\frac{1}{3(1+Ts)}(V_{ga}+V_{gb}+V_{gc}) \tag{7}$$

The internal voltages of the grid-forming inverter are controlled to be three-phase balanced, as described by (8).

$$E_a=E_b=E_c=E\ ,\ \delta_a=\delta_b+\frac{2}{3}\pi=\delta_c-\frac{2}{3}\pi=\delta \tag{8}$$

D. Distribution Network Solution

The open-source software GridLAB-D was selected as the distribution network solver [20]. The network and loads in GridLAB-D are modeled using a per phase representation, allowing a complete representation of line and load unbalances. The power flow solution used in GridLAB-D is an extension of the current injection method described in [27].

V. Model Validation in Small Systems

To verify the proposed models of grid-following and grid-forming inverters, the three-phase, electromechanical simulation results from GridLAB-D are compared to the electromagnetic simulation results from PSCAD [28]. Moreover, field test results from the CERTS/AEP microgrid are used to validate the grid-forming inverter model.

A. Grid-Following Inverter

Grid-following control aims to track P_{ref} and Q_{ref}, so a step change in P_{ref} is used to validate the proposed grid-following inverter model. In this simulation, a 100 kW grid-following inverter is connected to an infinite bus through a short distribution line of 0.0217 + j0.0223 pu, and P_{ref} is changed from 0.5 pu to 1 pu at 0.1 s. Fig. 10 (a)–(c) shows GridLAB-D and PSCAD simulation results. It can be seen in Fig. 10 (a) that the inverter output currents i_{gda} and i_{gqa} respond quickly to the change in current references and reach a steady state within 0.1 s. Fig. 10 (b) and (c) show the inverter internal voltages e_{da} and e_{qa}.

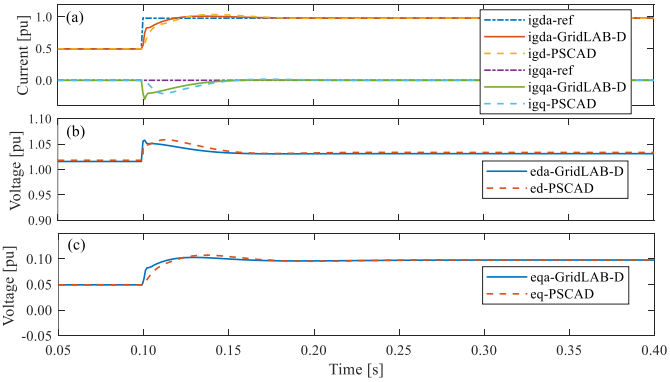

Fig. 10. GridLAB-D and PSCAD simulation of a grid-following inverter.

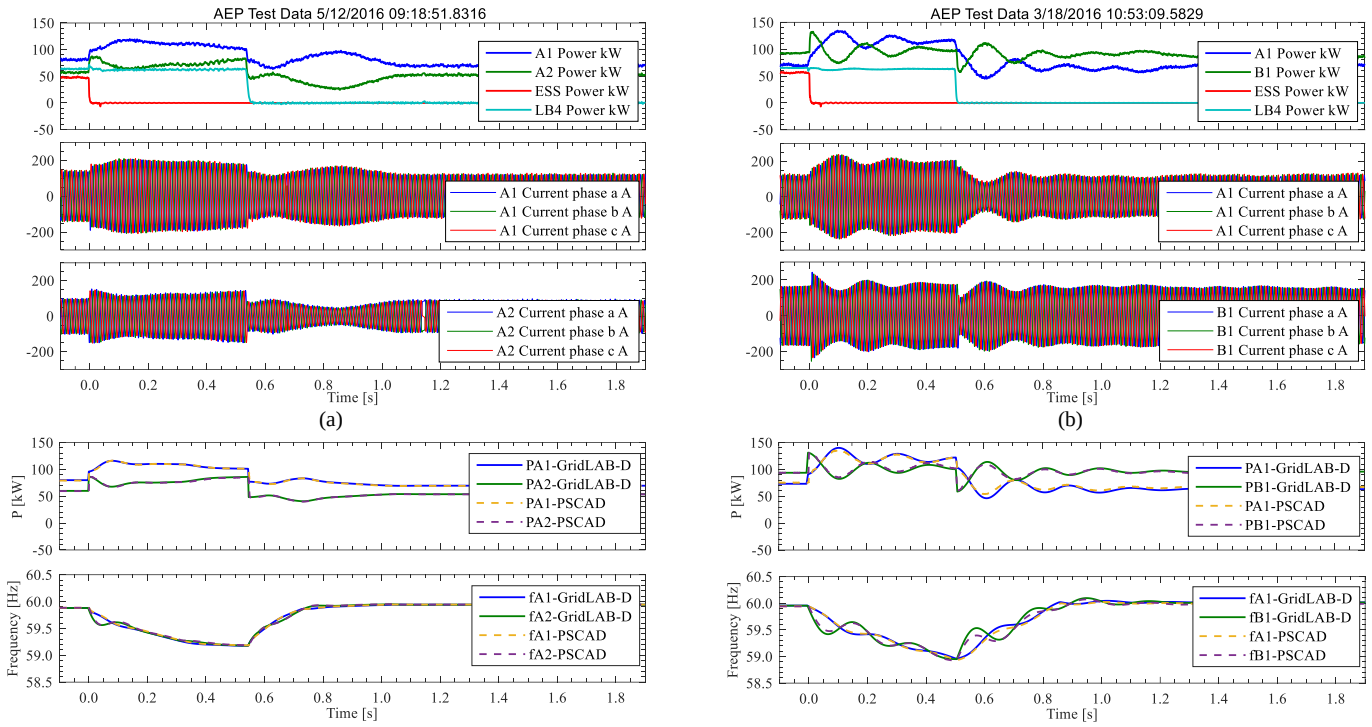

Fig. 11. Field test and simulation results of two under-frequency load shedding events from the CERTS/AEP microgrid. (a) and (c): Load shedding in a purely inverter-based microgrid. (b) and (d): Load shedding in an inverter and generator mixed microgrid.

The simulation results from GridLAB-D are slightly different than the simulation results from PSCAD. This is because in electromagnetic simulations, the fast-responding current control loop interacts with the dynamics of the inverter filter inductance and line impedance, but the dynamics of filter inductance and line impedance are ignored in the electromechanical simulation, resulting in the difference in the simulation results.

B. Grid-Forming Inverter

Given the fact that both *P-f* droop control and overload mitigation control are activated during the load shedding process, two under-frequency load shedding field test results from the CERTS/AEP microgrid were used to validate the proposed grid-forming inverter model. The first test is under-frequency load shedding in a purely grid-forming inverter-based microgrid, and the second test is under-frequency load shedding in a grid-forming inverter and synchronous generator mixed microgrid. Fig. 12 shows the one-line diagram of the reduced CERTS/AEP microgrid, and Fig. 11 (a) and (b) present the two field test results.

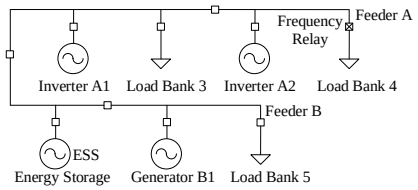

Fig. 12. One-line diagram of the reduced CERTS/AEP microgrid

In the first test, grid-forming inverters A1 (100kW), A2 (60 kW) and energy storage system (ESS, 100 kW) work together in islanded mode, and the tripping of the ESS results in the output power of A1 and A2 exceeding their maximum power outputs. Therefore, their overload mitigation controllers (as shown in Fig. 9 (b)) are activated to reduce the frequency rapidly. The frequency relay installed at Load Bank 4 detects the under-frequency event and trips Load Bank 4, resulting in the survival of the microgrid. Fig. 11 (c) shows both GridLAB-D and PSCAD simulation results. It can be seen that the GridLAB-D simulation results match the PSCAD simulation results very well, even though they use fundamentally different simulation approaches. The simulation results are also very similar to the field test results. Although detailed ac waveforms no longer exist in GridLAB-D simulation, it can accurately simulate the dynamic process of under-frequency load shedding. The second test is similar to the first but A2 is replaced by synchronous generator B1 (93 kW). Fig. 11 (b) and (d) show that the GridLAB-D simulation results, PSCAD simulation results, and field test results still match well. The slight difference between GridLAB-D and PSCAD simulation results shown in Fig. 11 (d) can be attributed to the difference in the synchronous generator models used in GridLAB-D and PSCAD.

Both under-frequency load shedding tests have verified the proposed modeling approach for grid-forming inverters. Detailed explanations and parameters of the two field test results are provided in [26].

VI. Simulation in a Large-Scale, Three-Phase Unbalanced Distribution System

To evaluate the feasibility of the proposed inverter models for the transient stability simulation of large-scale, three-phase unbalanced distribution systems, the prototypical distribution feeder, R3-12.47-3, developed at Pacific Northwest National

Laboratory was selected as the studied system [29]. The feeder has 5,252 nodes, including 2,002 nodes at the primary voltage side and 3,250 nodes at the secondary voltage side, representing a typical full-size distribution feeder in a heavily populated suburban area in North America. The rated voltage on the primary side is 12.47 kV, and the rated voltages on the secondary side are 480 V and 120 V. The total load is around 8 MW and has a power factor of 0.9.

The following modifications are made to conduct the transient stability simulation. (a) The substation voltage source is disconnected to examine the capability of the DERs to maintain the stability of the islanded distribution system. (b) Three 2 MW diesel generators, each having an *H* of 1 s, are installed in the feeder. The generator model is based on the work in [6], but additional Q-V droop control is modeled to avoid circulating reactive power during parallel operations. (c) Ten 500 kW utility-scale inverter-based DERs are installed in the feeder. The inverters can be either grid-following or grid-forming controlled, and the controller parameters are provided in Table I and II in the Appendix. (d) Approximately 25% of the loads are equipped with under-frequency load shedding devices with a load shedding frequency of 59 Hz and time delay of 0.05s. (e) The switching actions of regulators and shunt capacitors are ignored due to their slow responses.

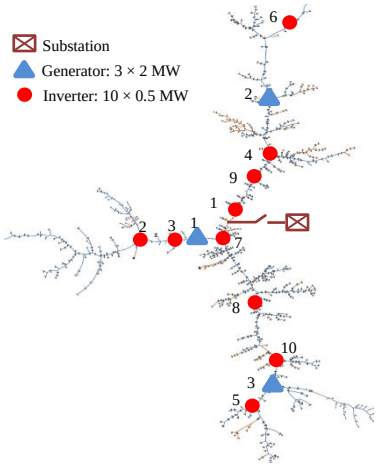

Fig. 13. The studied 5,252 node islanded distribution system.

Fig. 13 shows the studied distribution feeder and the locations of the DERs. The initial condition is that the three synchronous generators are each dispatched to output around 1.8 MW, and the ten inverters are categorized as three groups: Inverter 1–3 each output 100 kW, Inverter 4–8 each output 300 kW, and Inverter 9–10 each output 500 kW. Note that Inverter 9 and 10 are dispatched at their maximum power outputs. The voltage set points of generators and grid-forming inverters are set at 1 pu. The grid-following inverters generate power at unity power factor. Three cases are simulated as follows. In Case A, Generator 1 is tripped and all inverters are grid-following controlled. In Case B, Generator 1 is tripped and all inverters are grid-forming controlled. In Case C, Generator 2 is tripped following Case B.

A. Loss of One Generator with all Grid-Following Inverters

Fig. 14 and Fig. 15 show the simulation results for Case A. The tripping of Generator 1 results in a significant frequency oscillation in the islanded distribution system, triggering under-frequency load shedding.

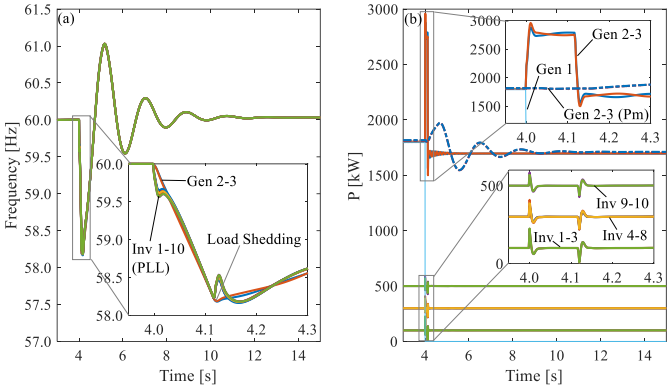

Fig. 14. Simulation results for Case A: (a) frequency and (b) active power.

In Fig. 14 (a), the frequencies of generators refer to their speeds, and the frequencies of inverters are measured by their PLLs. As shown in Fig. 14 (b), at the very beginning of the event both generators and inverters increase their output power to meet the loss of generation. This is because both generators and inverters behave as voltage sources behind reactances, and their internal voltages are constant initially. However, the grid-following controllers quickly regulate the output power of the inverters back to their power references by changing the inverter internal voltages rapidly, as explained in Section V-A. Therefore, Generator 2 and 3 have to take all the output power of Generator 1, resulting in a significant imbalance between generators' mechanical power and electrical power between 4.0 s to 4.1 s, as shown in Fig. 14 (b). This imbalance forces the speed to drop, as explained in Section II. The frequency transient after load shedding is caused by the dynamic response of generators' governors.

Fig. 15 (a) and (b) show the three-phases voltages of all the nodes at the primary voltage side, and the output reactive power of generators and inverters, respectively. The node voltages range from 0.948 pu to 0.983 pu before the event, and from 0.923 pu to 0.981 pu after the event. During load transients, the voltages drop to 0.750 pu and jump to 1.065 pu due to the response of the generators' exciters. The voltage profile is relatively poor because only the generators control the system voltage, resulting in a weak islanded system. The tripping of Generator 1 further reduces the stiffness of the system. The grid-following inverters are controlled as current sources, so they do not control the voltage.

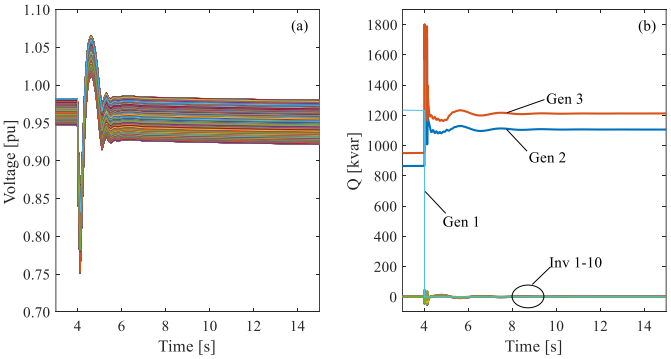

Fig. 15. Simulation results for Case A: (a) voltages and (b) reactive power.

B. Loss of One Generator with all Grid-Forming Inverters

Fig. 16 and Fig. 17 show the simulation results for the same loss of generation event but with all inverters being grid-forming controlled. As shown in Fig. 16 (a), the frequency nadir is significantly improved compared to the results for Case A, and under-frequency load shedding is avoided. In Fig. 16 (a), the frequencies of generators refer to their speeds, and the frequencies of inverters are obtained from their controllers (as shown in Fig. 9 (b)). The improvement in the frequency nadir is caused by the grid-forming inverters quickly increasing their output power after the event because of their voltage source characteristics, thereby resulting in a much smaller unbalance between the mechanical power and electrical power of generators during load transients, as shown in Fig. 16 (b).

As shown in Fig. 16 (a), the frequencies are different between 4.0 s to 4.2 s, and can be divided into four groups. The initial frequency drop of Generator 2–3 is decided by their inertia time constants *H*, and the frequency drop of inverters is decided by their controllers. As shown in Fig. 16 (b), because Inverter 9 and 10 already output their maximum power before the event, their overload mitigation controllers are activated after the tripping of Generator 1, so their frequencies drop faster than the other inverters, as shown in Fig. 16 (a). In contrast, the output power of Inverter 1–3 do not exceed their maximum outputs during the load transient, so their frequencies are only governed by the *P-f* droop controllers and are the highest among all inverters. The output power of Inverter 4–8 exceed their maximum power outputs between 4.07 s to 4.17 s, as shown in Fig. 16 (b), so their frequencies are between those of the other two groups of inverters. All frequencies reach the same value in the steady state. The frequency drop in the steady state is decided by the droop slope of the generators' governors and the inverters' *P-f* droop controllers, which is set at 1% for both in this study.

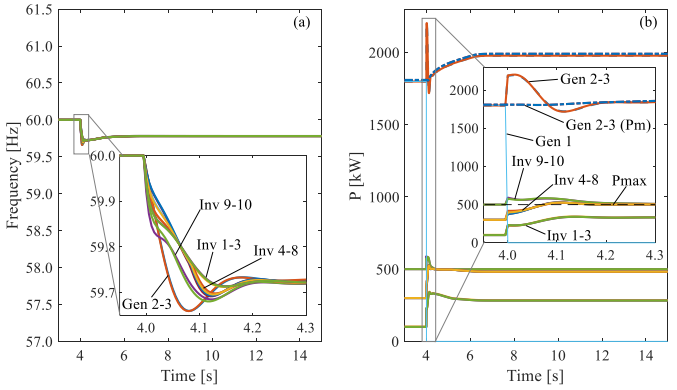

Fig. 16. Simulation results for Case B: (a) frequency and (b) active power.

Fig. 17 (a) and (b) show the three-phases voltages of all the nodes at the primary voltage side, and the output reactive power of generators and inverters, respectively. The node voltages range from 0.966 pu to 0.992 pu before the event, and from 0.953 pu to 0.991 pu after the event. The voltage drops to 0.944 pu during load transients. The voltage profile is significantly improved compared to the results for Case A, especially during load transients. This is because the internal voltages of grid-forming inverters are almost constant during the event and they autonomously increase necessary output reactive power to maintain the voltage, as shown in Fig. 17 (b).

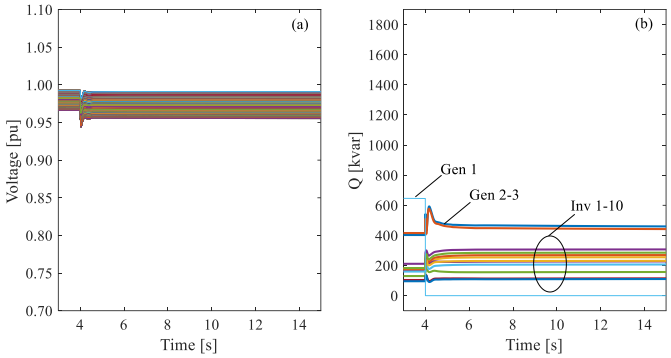

Fig. 17. Simulation results for Case B: (a) voltages and (b) reactive power.

C. Loss of Two Generators with all Grid-Forming Inverters

In case C, Generator 2 is tripped at 15 s following Case B. The loss of two generators results in insufficient generation of the islanded system (7 MW generation versus 8 MW load). Therefore, both generators and inverters are overloaded, and the overload mitigation controllers of inverters are activated to reduce the system frequency, thereby triggering under-frequency load shedding. The results in Fig. 18 (a) and (b) are similar to the load shedding results for CERTS/AEP microgrid shown in Fig. 11, but the simulation is conducted in a large-scale distribution system that has thousands of nodes. Note that the under-frequency load shedding in Case C is different from that in Case A. In Case A, the inverters still have sufficient generation to supply all the loads, but the grid-following control cannot autonomously increase the output power of inverters to meet the load change; therefore, load shedding is triggered due to the frequency transient of the generators. The under-frequency load shedding in Case C is caused by the overload situation of the entire islanded distribution system, in which some loads have to be tripped to guarantee the survival of the system.

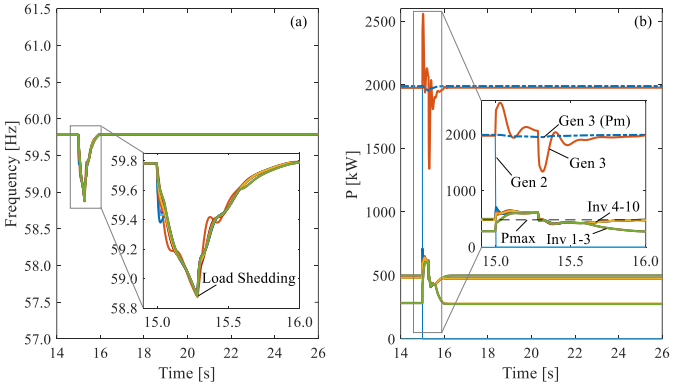

Fig. 18. Simulation results for Case C: (a) frequency and (b) active power.

The three cases above demonstrate the feasibility of using the proposed inverter models for transient stability simulation of large-scale distribution systems. Simulation results show that the use of grid-forming inverters can improve the voltage and frequency transient stability of distribution systems.

VII. Conclusion

The emerging generation of distribution systems is expected to have the capability to allow portions of, or all the distribution feeder to work in islanded modes to improve system resilience. To examine the transient stability of such islanded distribution systems that feature high penetration of inverter-based DERs, this paper develops three-phase, electromechanical models for both grid-following and grid-forming inverters, and integrates them into a three-phase unbalanced distribution network solver, enabling transient stability simulation of large-scale distribution systems. The inverter models faithfully represent the control strategies used by typical grid-following and grid-forming inverters. The proposed inverter models are validated against electromagnetic simulations and field test data from the CERTS/AEP microgrid testbed, and evaluated in an islanded 5,252 node distribution feeder that has multiple synchronous generator-based and inverter-based DERs in the GridLAB-D simulation environment. The simulation verifies the effectiveness of the proposed inverter models for large-scale distribution systems study. Study results show that compared to grid-following inverters, the high penetration of grid-forming inverters can significantly improve the voltage and frequency transient stability of distribution systems.

VIII. Appendix

TABLE I.
GRID-FOLLOWING CONTROLLER PARAMETERS.

k_{pc}	k_{ic}	k	k_{pPLL}	k_{iPLL}
0.05 pu	5 pu	0.5 pu	50 pu	1,000 pu/s

TABLE II.
GRID-FORMING CONTROLLER PARAMETERS.

m_p	m_q	T	ω_0	k_{pv}
3.77 rad/s	0.05 pu	0.01 s	376.99 rad/s	0 pu
k_{iv}	k_{ppmax}	k_{ipmax}	P_{max}	P_{min}
5.86 pu/s	3 pu	60 pu/s	1 pu	0 pu

IX. References

[1] B. Kroposki *et al.*, "Achieving a 100% Renewable Grid: Operating Electric Power Systems with Extremely High Levels of Variable Renewable Energy," *IEEE Power and Energy Magazine,* vol. 15, no. 2, pp. 61-73, 2017.

[2] R. H. Lasseter, "Smart Distribution: Coupled Microgrids," *Proceedings of the IEEE,* vol. 99, no. 6, pp. 1074-1082, 2011.

[3] D. T. Ton and W. P. Wang, "A More Resilient Grid: The U.S. Department of Energy Joins with Stakeholders in an R&D Plan," *IEEE Power and Energy Magazine,* vol. 13, no. 3, pp. 26-34, 2015.

[4] K. P. Schneider, F. K. Tuffner, M. A. Elizondo, C. C. Liu, Y. Xu, and D. Ton, "Evaluating the Feasibility to Use Microgrids as a Resiliency Resource," *IEEE Transactions on Smart Grid,* vol. 8, no. 2, pp. 687-696, 2017.

[5] P. Kundur, *Power System Stability and Control*. McGraw-Hill Education, 1994.

[6] M. Elizondo, F. Tuffner, and K. Schneider, "Three-phase unbalanced transient dynamics and powerflow for modeling distribution systems with synchronous machines," in *2016 IEEE Power and Energy Society General Meeting (PESGM)*, 2016, pp. 1-1.

[7] D. Ramasubramanian, Z. Yu, R. Ayyanar, V. Vittal, and J. Undrill, "Converter Model for Representing Converter Interfaced Generation in Large Scale Grid Simulations," *IEEE Transactions on Power Systems,* vol. 32, no. 1, pp. 765-773, 2017.

[8] M. E. Elkhatib, W. Du, and R. H. Lasseter, "Evaluation of Inverter-based Grid Frequency Support using Frequency-Watt and Grid-Forming PV Inverters," in *2018 IEEE Power & Energy Society General Meeting (PESGM)*, 2018, pp. 1-5.

[9] B. J. Pierre *et al.*, "Bulk Power System Dynamics with Varying Levels of Synchronous Generators and Grid-Forming Power Inverters," in *the 46th IEEE Photovoltaic Specialists Conference*, Chicago, Illinois, USA, 2019.

[10] W. H. Kersting, *Dystribution Systems Modeling and Analysis*, 3rd ed. Boca Raton, FL, USA: CRC, 2012.

[11] "Impact of Inverter Based Generation on Bulk Power System Dynamics and Short-Circuit Performance," IEEE PES Industry Technical Support Task Force, PES-TR68, 2018, [Online]. Available: https://resourcecenter.ieee-pes.org/technical-publications/technical-reports/PES_TR_7-18_0068.html.

[12] D. Pattabiraman, R. H. Lasseter, and T. M. Jahns, "Comparison of Grid Following and Grid Forming Control for a High Inverter Penetration Power System," in *2018 IEEE Power & Energy Society General Meeting (PESGM)*, 2018, pp. 1-5.

[13] G. Denis, T. Prevost, M. S. Debry, F. Xavier, X. Guillaud, and A. Menze, "The Migrate project: the challenges of operating a transmission grid with only inverter-based generation. A grid-forming control improvement with transient current-limiting control," *IET Renewable Power Generation,* vol. 12, no. 5, pp. 523-529, 2018.

[14] M. C. Chandorkar, D. M. Divan, and R. Adapa, "Control of parallel connected inverters in stand-alone AC supply systems," in *Industry Applications Society Annual Meeting, 1991., Conference Record of the 1991 IEEE*, 1991, pp. 1003-1009 vol.1.

[15] P. Piagi and R. H. Lasseter, "Autonomous control of microgrids," in *2006 IEEE Power Engineering Society General Meeting*, 2006, p. 8 pp.

[16] B. B. Johnson, S. V. Dhople, A. O. Hamadeh, and P. T. Krein, "Synchronization of Parallel Single-Phase Inverters With Virtual Oscillator Control," *IEEE Transactions on Power Electronics,* vol. 29, no. 11, pp. 6124-6138, 2014.

[17] Q. Zhong, "Virtual Synchronous Machines: A unified interface for grid integration," *IEEE Power Electronics Magazine,* vol. 3, no. 4, pp. 18-27, 2016.

[18] W. Du *et al.*, "A Comparative Study of Two Widely Used Grid-Forming Droop Controls on Microgrid Small Signal Stability," *IEEE Journal of Emerging and Selected Topics in Power Electronics,* pp. 1-1, 2019.

[19] R. H. Lasseter *et al.*, "CERTS Microgrid Laboratory Test Bed," *IEEE Transactions on Power Delivery,* vol. 26, no. 1, pp. 325-332, 2011.

[20] D. P. Chassin, K. Schneider, and C. Gerkensmeyer, "GridLAB-D: An open-source power systems modeling and simulation environment," in *2008 IEEE/PES Transmission and Distribution Conference and Exposition*, 2008, pp. 1-5.

[21] A. Yazdani and R. Iravani, *Voltage-Sourced Converters in Power Systems : Modeling, Control, and Applications*. Wiley-IEEE Press, 2010.

[22] GE Energy Consulting, PSLF Software, 2018 [Online] Available: https://www.geenergyconsulting.com/practice-area/software-products/pslf

[23] SIEMENS, PSS/E Software, 2018 [Online] Available: https://new.siemens.com/global/en/products/energy/services/transmission-distribution-smart-grid/consulting-and-planning/pss-software/pss-e.html

[24] A. Hoke *et al.*, "Setting the Smart Solar Standard: Collaborations Between Hawaiian Electric and the National Renewable Energy Laboratory," *IEEE Power and Energy Magazine,* vol. 16, no. 6, pp. 18-29, 2018.

[25] D. Duckwitz and B. Fischer, "Modeling and Design of df/dt-Based Inertia Control for Power Converters," *IEEE Journal of Emerging and Selected Topics in Power Electronics,* vol. 5, no. 4, pp. 1553-1564, 2017.

[26] W. Du, R. H. Lasseter, and A. S. Khalsa, "Survivability of Autonomous Microgrid During Overload Events," *IEEE Transactions on Smart Grid,* vol. 10, no. 4, pp. 3515-3524, 2019.

[27] P. A. N. Garcia, J. L. R. Pereira, S. Carneiro, V. M. d. Costa, and N. Martins, "Three-phase power flow calculations using the current injection method," *IEEE Transactions on Power Systems,* vol. 15, no. 2, pp. 508-514, 2000.

[28] Manitoba HVDC Research Centre, PSCAD Software, 2019 [Online] Available: https://hvdc.ca/pscad/

[29] K. P. Schneider, Y. Chen, D. P. Chassin, R. Pratt, D. Engel, and S. Thompson, "Modern Grid Initiative Distribution Taxonomy Final Report," Pacific Northwest National Laboratory, PNNL-18035, 2008.